Journal of ELECTRONIC MATERIALS, Vol. 39, No. 9, 2010
DOI: 10.1007/s11664-009-1034-6

Improved Thermoelectric Performance of Higher Manganese Silicides with Ge Additions

A.J. ZHOU,[1,2] T.J. ZHU,[1] X.B. ZHAO,[1,3] S.H. YANG,[1] T. DASGUPTA,[2] C. STIEWE,[2] R. HASSDORF,[2] and E. MUELLER[2]

1.—State Key Laboratory of Silicon Materials, Department of Materials Science and Engineering, Zhejiang University, Hangzhou 310027, China. 2.—Institute of Materials Research, German Aerospace Center (DLR), 51147 Köln, Germany. 3.—e-mail: zhaoxb@zju.edu.cn

Polycrystalline higher manganese silicides (HMS) with Ge additions were prepared by induction melting followed by hot-pressing. The phase structures and microstructure of the pellets were investigated, and their thermoelectric properties were measured from room temperature to 650°C. It was found that the solubility of Ge in HMS was limited to around 1.6%, beyond which an extra phase of Si_yGe_{1-y} appeared. The electrical conductivity was continuously enhanced by Ge additions, while the Seebeck coefficient was slightly decreased. The thermal conductivity showed first a decreasing then an increasing relationship with increasing Ge additions. The HMS cells, mainly along the *c*-axis, were remarkably enlarged by the substitution of Ge, which probably resulted in the enhancement of phonon scattering due to an increased number of defects, reducing the phonon thermal conductivity. The dimensionless figure of merit of the optimized HMS polycrystals was improved by more than 30% compared with the pure HMS material.

Key words: Higher manganese silicides, Ge additions, thermoelectric properties, hot-pressing

INTRODUCTION

Higher manganese silicides (HMS) are intermetallic compounds with composition $MnSi_{1.71–1.75}$. They have attracted increasing attention for potential application in thermoelectric (TE) devices providing direct conversion from heat to electricity as power generators, or reversely as coolers.[1–6] The advantages of HMS as TE materials include the low cost of the raw materials, their environmental friendliness, and their good thermal and chemical stability at high temperature.[7] To date, much work has focused on melt-grown single crystals[8–11] showing anisotropic transport properties, which has to be taken into consideration for practical applications. In the last few years, attention has also been paid to HMS thin films.[12–14] However, reports on the TE properties of polycrystalline HMS are limited, mainly due to difficulties in obtaining a single phase. In the case of preparing HMS by mechanical alloying, the oxidation of Mn and Si loss[2,15] during ball-milling make it difficult to control the composition. Additionally, induction melting has also been used for the preparation of bulk HMS, being able to obtain the desired compositions.[3,16]

So far, compositional optimization by doping or substitution has mainly been used to tune the transport properties of HMS to improve their TE performance.[4] It was reported that Ge addition tripled the room-temperature figure of merit Z of grown HMS single crystals along the *c*-axis to 0.7×10^{-3} K^{-1}.[11] Ge addition was found to considerably change the microstructure and the ratio of MnSi striations precipitated along the *c*-plane of HMS, which in turn changed the electrical properties and thermal conductivity in a favorable way. However, the temperature dependence of the TE properties was not reported for the Ge-added single-crystal HMS. In this work, we prepared polycrystalline HMS with Ge additions by induction melting and subsequent hot-pressing. The effects of Ge

(Received July 10, 2009; accepted November 30, 2009; published online December 24, 2009)

additions on the phase structures and microstructure were investigated, and TE properties from room temperature to 650°C are reported.

EXPERIMENTAL PROCEDURES

Ingots of $Mn(Si_{1-x}Ge_x)_{1.733}$ (x = 0%, 0.05%, 0.2%, 0.8%, 1.6%, and 2%) were prepared by induction melting of Mn (99.99%), Si (99.999%), and Ge (99.999%). The Mn flakes were chemically cleaned with diluted HNO_3 (4% weight ratio) before being weighed, in order to remove visible oxidation layers. No further purification was carried out for the pure Si and Ge raw ingots. Stoichiometrically weighed pure elements were loaded into a coverable graphite crucible and then moved into the chamber of the induction furnace. The melting was carried out at 1350°C for 5 min in argon. The temperature was measured with an infrared thermometer through a glass window in the chamber. The as-melted ingots were then ground with an agate mortar and pestle and sieved into powders with a maximum size of 0.04 mm. These powders were subsequently charged into a graphite die of 12.7 mm diameter and hot-pressed under 100 MPa at 900°C for 60 min in vacuum.

Phase purity and crystal structure were studied by x-ray diffraction (XRD) by using a Siemens D5000 diffractometer using Cu K_α radiation (λ = 1.5406 Å). Morphologies and microstructure were observed by scanning electron microscopy (SEM, Zeiss ULTRA-55) and optical microscopy. For the observation of MnSi striations, the pellets were chemically etched for 60 s at room temperature using an etching solution ($HF:HNO_3:H_2O_2$ = 1:6:13 volume ratio) after being polished.[11] Electrical conductivity, σ, measurements were performed by the standard four-probe direct-current (DC) method. The potential difference ΔU and temperature difference ΔT between the hot and cold side of the sample were measured with a home-built setup in vacuum from room temperature to 700°C. The Seebeck coefficient α was estimated by the equation $\alpha = \lim_{\Delta T \to 0} (\Delta U/\Delta T)$. The thermal conductivity was calculated by $\kappa = Dc_p\rho$, where ρ is the sample density measured using the Archimedes method, D is the thermal diffusivity, and c_p is the specific heat, measured using a Netzsch LFA-427 and Netzsch DSC-404, respectively. The uncertainty of the measurements was estimated to be $<5\%$ for σ and $<10\%$ for α and κ. The room-temperature Hall coefficient R_H was measured with a magnetic field change of 1.6 T and a current of around 6 mA. The carrier concentration n and the mobility μ_H were calculated from $n = 1/(eR_H)$ and $\mu_H = \sigma/(en)$, where e is the electron charge.

RESULTS AND DISCUSSION

Phase Structures of $Mn(Si_{1-x}Ge_x)_{1.733}$

Figure 1 shows XRD patterns of the Ge-added HMS after hot-pressing. One can see that all the

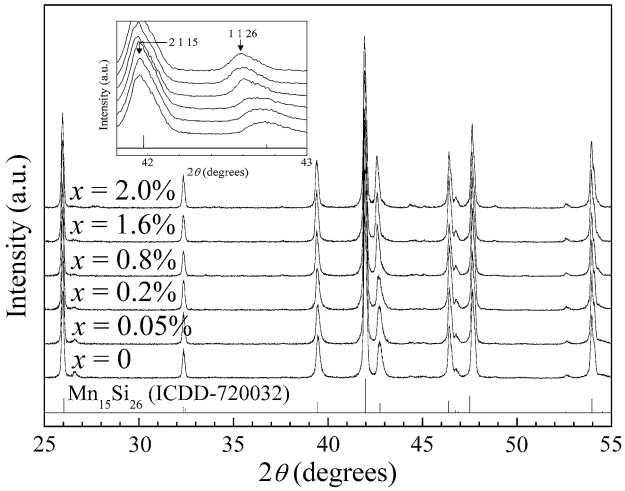

Fig. 1. XRD patterns of $Mn(Si_{1-x}Ge_x)_{1.733}$ after hot-pressing.

samples were mainly comprised of HMS phases. No impurity phases were observable. It is well known that HMS exist as several incommensurate phases such as Mn_4Si_7,[17] $Mn_{11}Si_{19}$,[18] $Mn_{15}Si_{26}$,[19] and $Mn_{27}Si_{47}$,[20] all of which belong to the same tetragonal crystal system deduced from the $TiSi_2$ structure with different numbers of subcells stacking along the c-axis. These incommensurate phases usually coexist with each other in a melted ingot and cannot be distinguished based on XRD results. For convenience in this paper, HMS phases are presented along with one of these incommensurable phases, $Mn_{15}Si_{26}$ (ICDD No. 72-0032), whose basic parameters were used for the calculation of cell parameters. In addition, the well-known MnSi phase that usually inherently exists in the HMS matrix was not identified due to its low content and special orientation.

As shown in the inset of Fig. 1, subtle peak shifts to lower angles were observed as the x value increased. This indicated the enlargement of the HMS unit cells and the increase of cell parameters due to Ge substitution. The calculated cell parameters of all samples are plotted in Fig. 2. One can see that the c value increased steadily at a much faster rate than a as the Ge content increased. This is due to the weaker interaction of the Si and Mn sublattices along the tetragonal c-axis,[4] which allows cell expansion in the c-direction much more easily than in the a-direction. A third-order polynomial fit to the c parameter showed a good match. Considering that the added Ge contributed only substitution for Si, one can estimate the solubility of Ge in the HMS structures to be ~1.6% (atomic), which is basically in accordance with the reported result.[21]

Microstructure of $Mn(Si_{1-x}Ge_x)_{1.733}$

It is well known that MnSi layers segregate along the c-plane of melted HMS due to incommensurability. Having a cubic structure, MnSi is known to

have metallic character, which is undesirable with respect to TE performance. Figure 3 shows optical-microscopy images of polished and etched pellets with different Ge contents. Due to the fact that MnSi can be etched relatively faster by HF, the distribution of MnSi striations can be easily observed. One can clearly see from Fig. 3 that, for a Ge content less than 0.2%, many MnSi linear striations still remain in HMS, being parallelly aligned in different grains with different orientations. When the Ge content is increased to 0.8%, the MnSi striations decreased significantly in quantity, and almost disappeared in the sample with $x = 1.6\%$. Meanwhile, the MnSi striations became more curved and nonparallel to each other, suggesting disturbance of the HMS structure. However, as further Ge was introduced ($x = 2\%$), some MnSi striations appeared again, which indicated excess Ge addition, that is, deviation from the phase composition. In other words, once the solubility limit of Ge is reached, any extra Ge will be alloyed with Si to form Si_yGe_{1-y}, which would result in the formation of more MnSi.

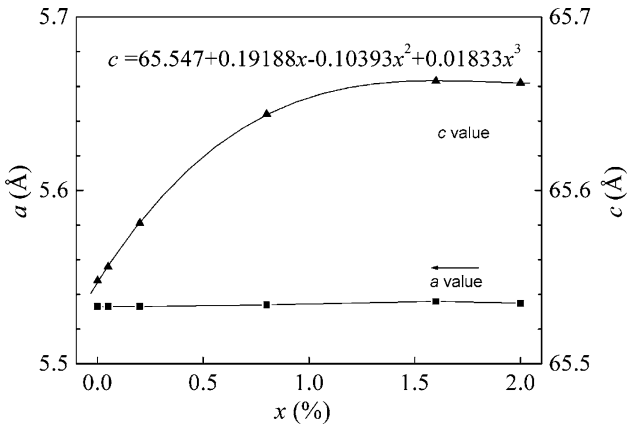

Fig. 2. Calculated cell parameters a (squares) and c (triangles) of $Mn(Si_{1-x}Ge_x)_{1.733}$.

The Si_yGe_{1-y} phase was actually observed, even in samples with Ge content below the maximum solubility. Figure 4 shows a typical SEM image of some Si_yGe_{1-y} inclusions. The bright areas were found to be randomly distributed in between the HMS grains with limited amount. Their composition was studied by energy-dispersive x-ray spectroscopy (EDX), and the y value was found to vary slightly in the range of 0.2 to 0.25 for different inclusions. Furthermore, some free Si and MnSi striations that formed during the cooling process were also observed in Fig. 4. The present observations

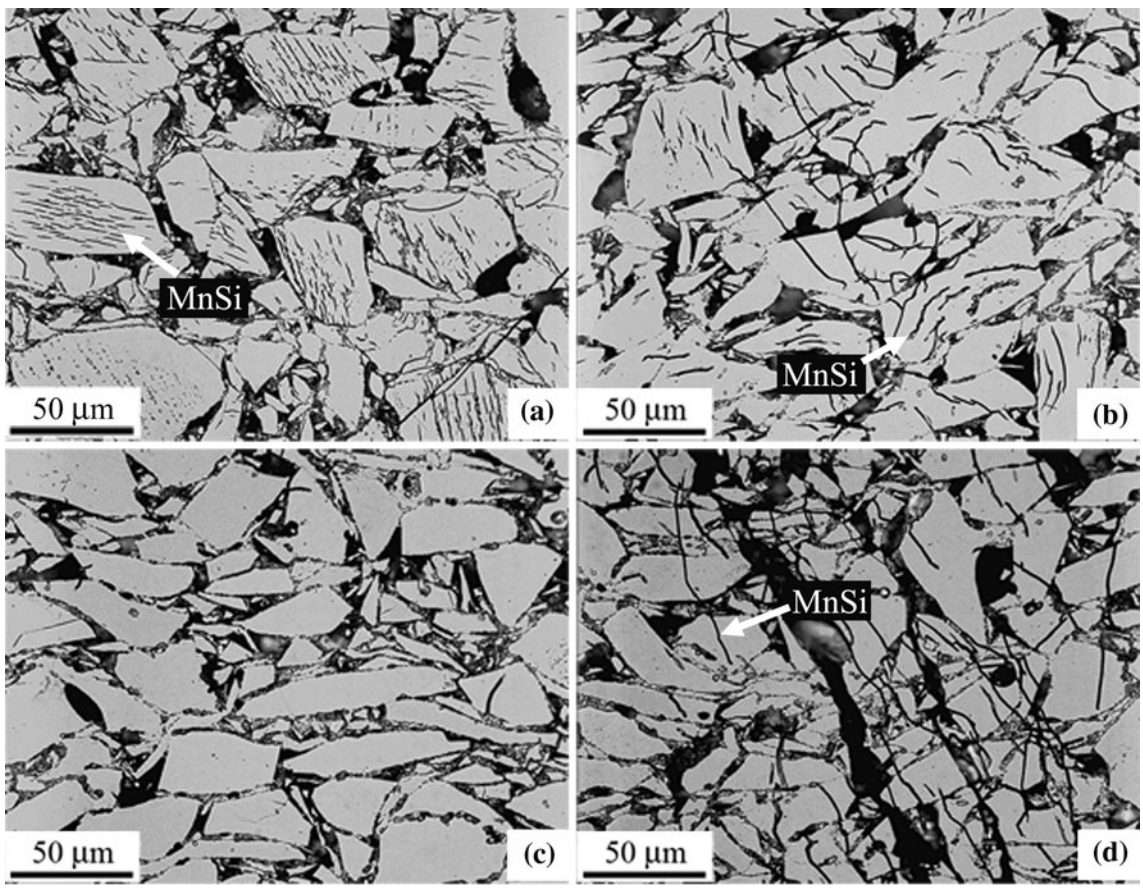

Fig. 3. Optical-microscopy images of $Mn(Si_{1-x}Ge_x)_{1.733}$ with (a) $x = 0.2\%$, (b) $x = 0.8\%$, (c) $x = 1.6\%$, and (d) $x = 2\%$.

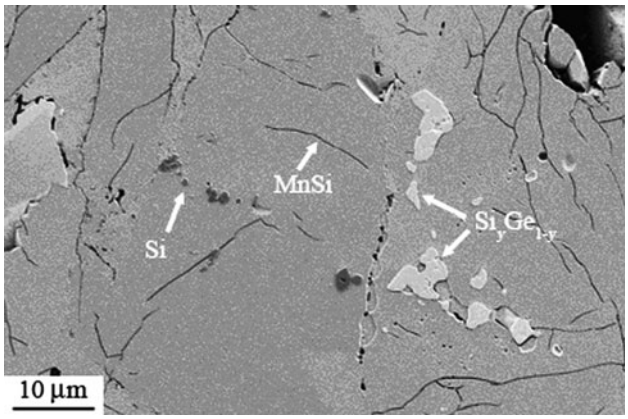

Fig. 4. Typical SEM image of Si_yGe_{1-y} inclusions in $Mn(Si_{1-x}Ge_x)_{1.733}$ with $x = 1.6\%$.

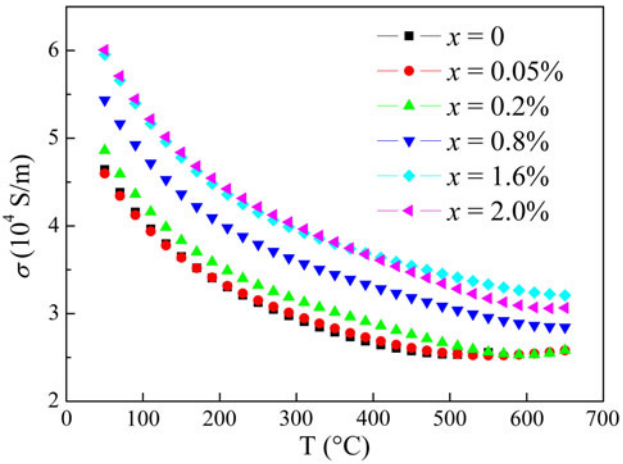

Fig. 5. Temperature dependence of the electrical conductivity σ of $Mn(Si_{1-x}Ge_x)_{1.733}$.

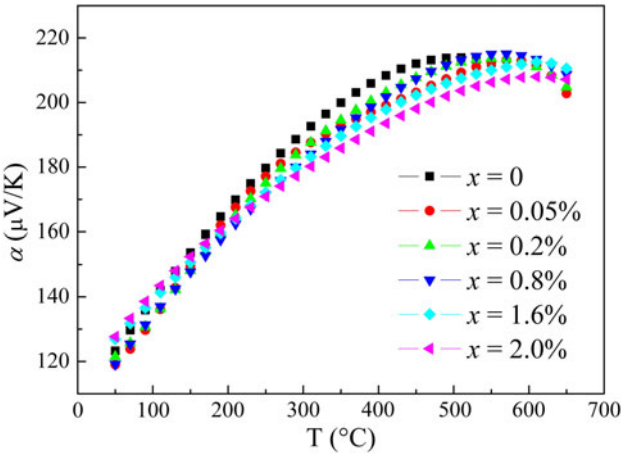

Fig. 6. Temperature dependence of the Seebeck coefficient α of $Mn(Si_{1-x}Ge_x)_{1.733}$.

showed different evolution of the microstructure in polycrystalline HMS compared with that in single-crystal HMS.[11] In the single crystals, a Ge doping level of around 0.13% was reported, below which the ratio of MnSi striations increased monotonically with Ge content. Above this limit ($x > 0.13\%$), the MnSi ratio decreased again and reached almost zero as x reached 0.53%. In this work, however, the MnSi content decreased continuously with increasing Ge content (up to 1.6%). This discrepancy could be firstly due to the different processes used for controlling the compositions and homogenizing the materials. In addition, due to the variety of crystal orientations, it is impossible to perform accurate quantitative analysis of the MnSi ratio in polycrystals based on microscopy observation. Nevertheless, both the literature and the present study reflect the same possibility that Ge addition could significantly influence the microstructure of HMS, especially the MnSi distribution, which may lead to changes in electrical and thermal properties.

TE Properties of $Mn(Si_{1-x}Ge_x)_{1.733}$

Temperature dependences of the electrical conductivity σ and the Seebeck coefficient α of the samples are shown in Figs. 5 and 6, respectively. As can be seen, pure HMS material exhibited the characteristics of a degenerate semiconductor, having a metal-like σ–T relationship below 500°C. With further increases of temperature, the intrinsic effect started to dominate, producing many more carriers over 500°C, and σ increased again. After the addition of Ge, the general conducting behavior of the samples was not changed. However, σ increased continuously with increasing Ge content until 1.6% and then remained unchanged as the Ge content reached 2%. In addition, the temperature corresponding to the minimum σ (intrinsic excitation) also increased with increasing Ge addition, indicating change of the carrier concentration in different samples. The Seebeck coefficient results suggested that all samples were p-type semiconductors, and the Ge additions had a decreasing effect on α. Compared with σ, however, the influence of Ge addition on α was much smaller. Room-temperature Hall measurements were carried out, and the results are listed in Table I. It can be seen that the carrier concentration was increased by Ge addition up to 1.6%, after which it decreased, while the mobility of the carriers did not change much. As a consequence, the increase of σ with increasing x

Table I. Electrical transport properties of $Mn(Si_{1-x}Ge_x)_{1.733}$ at 300 K

$Mn(Si_{1-x}Ge_x)_{1.733}$	$x = 0\%$	$x = 0.8\%$	$x = 1.2\%$	$x = 1.6\%$
σ (10^4 S m^{-1})	5.48	6.42	7.03	7.09
R_H (10^{-9} m^3 C^{-1})	4.19	3.82	3.31	3.62
n (10^{27} m^{-3})	1.50	1.64	1.89	1.72
μ_H (10^{-4} m^2 V^{-1} s^{-1})	2.28	2.44	2.32	2.57

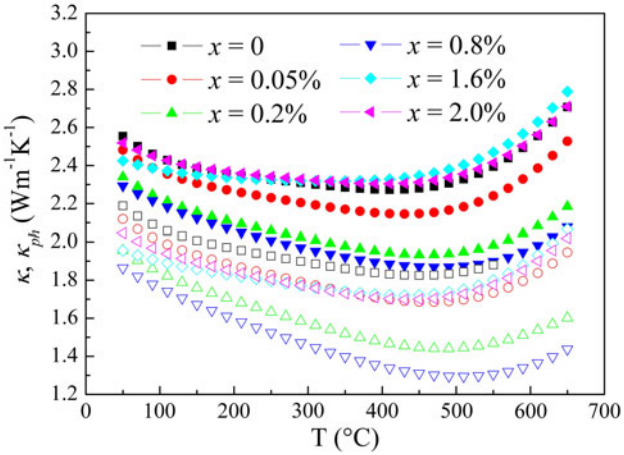

Fig. 7. Temperature dependences of the total thermal conductivity κ (filled) and the phonon contribution κ_{ph} (unfilled) of $Mn(Si_{1-x}Ge_x)_{1.733}$.

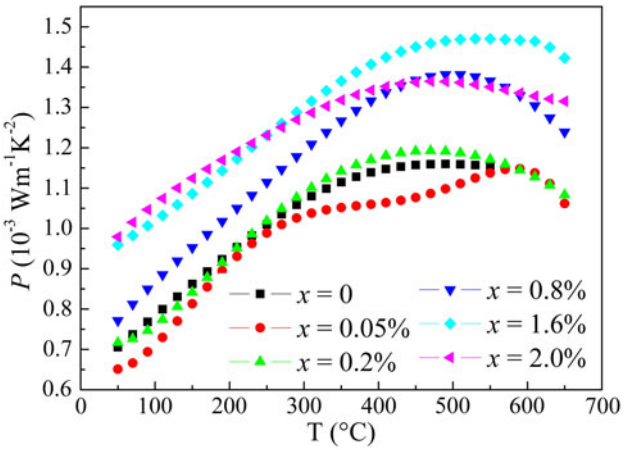

Fig. 8. Temperature dependence of the power factor P of $Mn(Si_{1-x}Ge_x)_{1.733}$.

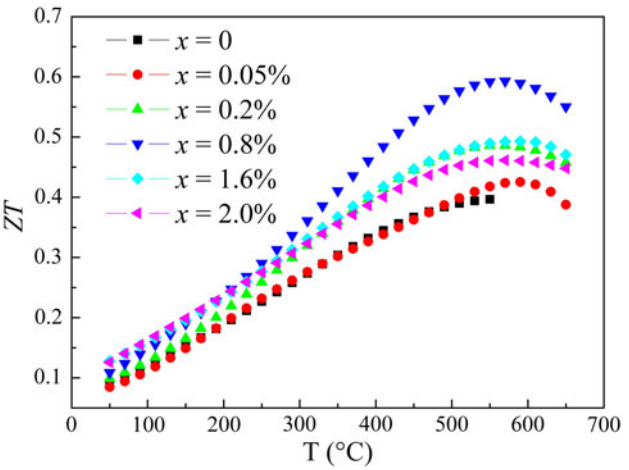

Fig. 9. Temperature dependence of the dimensionless figure of merit ZT of $Mn(Si_{1-x}Ge_x)_{1.733}$.

can be attributed to the increase of the carrier concentration by Ge addition. The increase of n was considered to be unusual because Ge substitution is an electron-neutral modification for HMS. However, some recent reports have indicated,[22,23] based on first-principle calculations of HMS band structures, that the distribution of the lower-lying conduction band, the band gap, and the density of states were strongly dependent on the atomic arrangement and positional modulation of the Si atoms, especially when stacking faults were created in the structures. In this work, based on the dramatic microstructure changes, the Ge additions might have disturbed the arrangement of the Si subcells, possibly forming stacking faults in the HMS and thus changing the density of states near the Fermi level. On the other hand, the microstructure changes relating to the MnSi striations and the presence of Si-Ge inclusions could also affect the conduction behavior in terms of the carrier mobility. More detailed, advanced microstructure observations are needed in order to clarify the effect of the microstructure changes on the transport properties.

Figure 7 shows the temperature dependences of the total thermal conductivity κ and the phonon contribution κ_{ph} of the pellets. The phonon contribution of the thermal conductivity was obtained by $\kappa_{ph} = \kappa - \kappa_e$, where κ_e is the electronic thermal conductivity calculated by $\kappa_e = L_0\sigma T$, where L_0 is the Lorenz number, approximately 2.44×10^{-8} V^2 K^{-2} for a degenerate semiconductor, and T is absolute temperature.[24] As seen in Fig. 7, the thermal conductivity κ was effectively decreased as Ge was introduced, and reached a minimum value as x reached 0.8%. With further Ge addition, κ increased again to the level of pure HMS. The phonon thermal conductivity κ_{ph} was found to be the dominant part of κ at lower temperatures, while at higher temperatures the electronic part started to increase significantly. Obviously, the decrease of κ_{ph} on Ge addition was responsible for the decrease of κ, because the electronic part κ_e should increase with increasing x according to Fig. 5. The decrease of κ_{ph} with increasing Ge content (up to 0.8%) was mainly due to enhanced phonon scattering by an increasing number of defects resulting from the substitution of Ge for Si. This is generally in accordance with the cell parameter changes in Fig. 2. On the other hand, the increase of κ for $x > 0.8\%$ can be attributed to the presence of Si-Ge phases, which possess much higher thermal conductivity than HMS.[25] The influence of the microstructural change of MnSi striations on the thermal conductivity is still not clear; however, it is believed that this would have a more significant effect on the electrical conductivity than on the thermal conductivity.

The power factor P ($P = \alpha^2\sigma$) and the dimensionless figure of merit ZT ($ZT = \alpha^2\sigma T/\kappa$) of the samples are plotted in Figs. 8 and 9, respectively. We can see that both the power factor and ZT were improved by Ge addition. The sample with $x = 1.6\%$ showed the

highest power factor among the samples. However, due to its low thermal conductivity, the highest ZT values were found in the sample with $x = 0.8\%$. The increase of ZT was more significant at higher temperature, because the temperatures corresponding to maximum σ and minimum κ were accordingly shifted to higher values as Ge was added. Compared with pure HMS, the ZT of Ge-added HMS was improved by more than 30%, with a maximum ZT value of 0.6 at 560°C, which is close to that of complex-doped HMS single crystals measured along the c-axis ($ZT_{max} = 0.7$).

CONCLUSIONS

TE performance of polycrystalline HMS was improved by slight substitution of Si atoms by Ge. Substitution of Ge resulted in the increase of cell parameters and the number of defects, which consequently tuned the electrical and thermal properties of HMS. The electrical conductivity increased continuously until the solubility limit of Ge was reached, while the Seebeck coefficient was only slightly decreased. The phonon thermal conductivity was remarkably reduced by the addition of up to 0.8% Ge, and then increased again as more Ge was added. As a result, a promising 30% improvement of ZT was achieved in this work. The prospect of using polycrystalline HMS instead of single-crystal HMS materials for future commercial applications could benefit from their more economical and flexible production processes and comparable TE performance.

ACKNOWLEDGEMENTS

The authors would like to thank Mr. W. Schönau from the Institute of Materials Research, German Aerospace Center (DLR) for thermal conductivity measurement. This work was supported by the National Science Foundation of China (Grant No. 50731006), the National Basic Research Program of China (Grant No. 2007CB607502), and the Sandwich Fellowship of the German Academic Exchange Service (DAAD).

REFERENCES

1. V.E. Borisenko, ed., *Semiconducting Silicides* (Berlin: Springer, 2000).
2. M. Umemoto, Z.G. Liu, R. Omatsuzawa, and K. Tsuchiya, *Mater. Sci. Forum* 342–346, 918 (2000).
3. A.J. Zhou, T.J. Zhu, H.L. Ni, Q. Zhang, and X.B. Zhao, *J. Alloys Compd.* 455, 255 (2008).
4. M.I. Fedorov and V.K. Zaitsev, *Thermoelectrics Handbook*, ed. D.M. Rowe (New York: CRC, 2005), p. 31.
5. Z.M. Wang, Y.D. Wu, and Y.J. He, *Int. J. Mod. Phys. B* 18, 87 (2004).
6. Z.M. Wang, Y.D. Wu, and Y.J. He, *Int. J. Mod. Phys. B* 18, 2279 (2004).
7. M.I. Fedorov, V.K. Zaitsev, F.Y. Solomkin, and M.V. Vedernikov, *Tech. Phys. Lett.* 23, 602 (1997).
8. I. Kawasumi, M. Sakata, I. Nishida, and K. Masumoto, *J. Mater. Sci.* 16, 355 (1981).
9. I. Kawasumi, M. Sakata, I. Nishida, and K. Masumoto, *J. Cryst. Growth* 49, 651 (1980).
10. T. Kojima, I. Nishida, and M. Sakata, *J. Cryst. Growth* 47, 589 (1979).
11. I. Aoyama, M.I. Fedorov, V.K. Zaitsev, F.Y. Solomkin, I.S. Eremin, A.Yu Samunin, M. Mukoujima, S. Sano, and T. Tsuji, *Jpn. J. Appl. Phys.* 44, 8562 (2005).
12. Q.R. Hou, W. Zhao, Y.B. Chen, D. Liang, X. Feng, H.Y. Zhang, and Y.J. He, *Phys. Status Solidi A* 204, 3429 (2007).
13. Q.R. Hou, W. Zhao, Y.B. Chen, D. Liang, X. Feng, H.Y. Zhang, and Y.J. He, *Appl. Phys. A* 86, 385 (2007).
14. Q.R. Hou, W. Zhao, H.Y. Zhang, Y.B. Chen, and Y.J. He, *Phys. Status Solidi A* 203, 2468 (2006).
15. I. Itoh and M. Yamada, *J. Electron. Mater.* 38, 925 (2009).
16. A.J. Zhou, X.B. Zhao, T.J. Zhu, Y.Q. Cao, C. Stiewe, R. Hassdorf, and E. Mueller, *J. Electron. Mater.* 38, 1072 (2009).
17. O.G. Karpinskii and B.A. Evseev, *Izv. Akad. Nauk SSSR, Neorg. Materialy.* 5, 525 (1969).
18. O. Shwomma, A. Preisinger, H. Nowotny, and A. Wittman, *Monatsh. Chem.* 95, 1527 (1964).
19. H.W. Knott, M.H. Mueller, and L. Heaton, *Acta Crystallogr.* 23, 549 (1967).
20. G. Zwilling and H. Nowotny, *Monatsh. Chem.* 102, 672 (1971).
21. E.N. Nikitin, A.F. Sidorov, V.I. Tarasov, and A.I. Zaslavskii, *Izv. Akad. Nauk SSSR, Neorg. Materialy* 6, 604 (1970).
22. D.B. Migas, V.L. Shaposhnikov, A.B. Filonov, V.E. Borisenko, and N.N. Dorozhkin, *Phys. Rev. B* 77, 075205 (2008).
23. M. Yuzuru, I. Dai, H. Kei, K. Tsuyoshi, and Y. Kunio, *Phys. Rev. B* 78, 214104 (2008).
24. R. Venkatasubramanian, E. Siivola, T. Colpitts, and B. O'Quinn, *Nature* 413, 597 (2001).
25. H. Stohr and W. Klemm, *Z. Anorg. Allgem. Chem.* 241, 305 (1954).